Nuclear Physics A561 (1993) 343–366
North-Holland

NUCLEAR
PHYSICS A

Excitation of low-lying states in ^{144}Nd by means of (e,e′) scattering

R. Perrino [a], N. Blasi [b], R. De Leo [c,d], M.N. Harakeh [e,f], C.W. de Jager [g], S. Micheletti [b], J. Mieremet [g], M. Pignanelli [b], V.Yu. Ponomarev [h], R.K.J. Sandor [e], H. de Vries [g]

[a] *Università di Lecce and Sezione INFN di Lecce, I-73100 Lecce, Italy*
[b] *Dipartimento di Fisica dell'Università di Milano and Sezione INFN di Milano, I-20133 Milano, Italy*
[c] *Dipartimento di Fisica dell'Università di Bari, I-70100 Bari, Italy*
[d] *Sezione INFN di Lecce, I-73100 Lecce, Italy*
[e] *Faculteit Natuurkunde en Sterrenkunde, Vrije Universiteit, De Boelelaan 1081, 1081 HV Amsterdam, The Netherlands*
[f] *Kernfysisch Versneller Instituut, Zernikelaan 25, 9747 AA Groningen, The Netherlands*
[g] *Nationaal Instituut voor Kernfysica en Hoge-Energie Fysica, Sectie K, P.O. Box 41882, 1009 DB Amsterdam, The Netherlands*
[h] *Laboratory of Theoretical Physics, Joint Institute for Nuclear Research Dubna, Head Post Office, P.O. Box 79, Moscow, Russian Federation*

Received 26 January 1993

Abstract

The low-lying states of ^{144}Nd have been investigated up to an excitation energy of 3.1 MeV by means of high-resolution inelastic electron scattering. Transition charge densities have been extracted for natural-parity states. The experimental data have been compared with the predictions of the quasiparticle–phonon model. The calculations show that both collective and single-particle degrees of freedom are important for describing the low-lying states of ^{144}Nd. A comparison of the present data with data for ^{142}Nd and ^{142}Ce emphasizes the role played by the two valence neutrons outside the $N = 82$ closed shell.

Key words: NUCLEAR REACTIONS ^{144}Nd(e,e′), $E = 112$–400 MeV; measured spectra, form factors. ^{144}Nd deduced L, J, π, $B(\lambda)$, transition charge densities. Comparison with microscopic quasiparticle–phonon model calculations. Fourier–Bessel analysis.

1. Introduction

Electron-scattering experiments on several isotopic chains of transitional nuclei in the rare-earth region have been performed in Saclay [1,2] on Sm, at MIT-Bates [3,4] on Ce, and at NIKHEF-K [5–7] on all stable even-A Nd isotopes. This renewed interest in electron-scattering experiments stems not only from the

established sensitivity of the probe to the static and dynamic nuclear structure properties, but also from the recent experimental developments which have resulted in a higher energy resolution. This permits the investigation of low-lying excitations of heavy nuclei, which were previously not accessible due to the high level density.

The data presented in this paper concern the excitation of low-lying states of ^{144}Nd by inelastic electron scattering performed at NIKHEF-K. The good resolution achieved in the experiment allowed one to extract cross sections for most states up to an excitation energy of ~ 3.1 MeV in the effective momentum range 0.5 to 2.15 fm^{-1}. Transition charge densities for these states were then obtained through a Fourier–Bessel analysis. The present experiment thus extends previous measurements [5–7] in the chain of even–even Nd isotopes. The nucleus ^{144}Nd represents an intermediate step in the shape transition from the spherical [5] nucleus ^{142}Nd, in which the $N = 82$ neutron shell is closed, to the transitional vibrational–rotational [6] nucleus ^{146}Nd. The Nd isotopic chain displays also a second transition to the deformed rotational [7] limit in ^{150}Nd, thus representing an interesting case of a transitional region in which the dynamic properties of the nuclei under investigation are strongly influenced by shape transitions.

The quasiparticle–phonon model [8] (QPM) has been shown [5] to be able to describe the excited states of ^{142}Nd, and, although it is in principle less suited [6] for transitional nuclei, it displayed some success in describing the structure of higher excited states of ^{146}Nd. The QPM is thus expected to give a good description of the excited states of ^{144}Nd, where only two particles are added to the closed neutron shell. While the low-lying excitations in the semi-magic nucleus ^{142}Nd are mainly due to proton configurations, the presence of two neutrons outside the closed $N = 82$ shell will introduce pairing neutron configurations into the lower excitation energies, presenting a more crucial test for the QPM. A transition similar to that occurring from ^{142}Nd to ^{144}Nd has been studied successfully within the framework of QPM for ^{140}Ce and ^{142}Ce in ref. [4] and ref. [3], respectively.

The experimental procedure and data analysis are similar to those in refs. [5–7]. In sect. 2 only those aspects will be discussed which differ from the earlier references; the data are also briefly compared with the results from a recent experiment of high-resolution inelastic proton and deuteron scattering [9]. The QPM theory is briefly sketched in sect. 3. In sect. 4 the QPM predictions are compared with the electron-scattering data. The conclusions are summarized in sect. 5.

2. Experimental method and data analysis

The experiments were performed at the electron scattering facility of NIKHEF-K [10]. The beam, produced by the medium-energy accelerator (MEA), had an

energy range of 100–400 MeV. The electrons scattered by the target were detected with the QDD spectrometer, characterized by an energy resolution better than 10^{-4} and a solid angle of 5.6 msr. An isotopically enriched ^{144}Nd target of 6.8 mg/cm^2 thickness, and with inhomogeneities estimated to be less than 1%, was used in transmission mode in order to get the optimum resolution (between 12 and 30 keV in the final spectra). The effective momentum transfer q_{eff} ranged from 0.5 to 2.15 fm^{-1}, where $q_{\text{eff}} = q(1 + 3Z\alpha/2E_i R_{\text{eq}})$ and R_{eq} is the equivalent nuclear radius, normally taken $1.12A^{1/3}$ fm. Two solid-angle acceptances with values of 0.4 and 5.6 msr were used. Dead-time losses were accounted for and the efficiencies of the spectrometer focal-plane wire chambers were evaluated as described in ref. [11]. Additional measurements on targets of boron nitride and ^{12}C, and of a number of known excited levels of ^{144}Nd were used to perform the energy calibration of the focal plane [12]. The measurements on the ^{12}C target were also used to establish normalizations. The uncertainty in the cross-section measurements was evaluated by adding quadratically the errors due to different sources. For the inelastic cross sections an additional error of 2.5% was introduced to account for normalization uncertainties. The systematic errors not accounted for in the normalization procedure were added to form the total error.

The cross sections of the observed peaks, extracted from the measured spectra, were corrected for dead-time losses and normalized by using the lineshape-fitting computer code ALLFIT [13]. This lineshape-fitting procedure, accounting for straggling, bremsstrahlung and Schwinger corrections to the peak shape, allowed the extraction of peaks up to 3.1 MeV excitation energy. Above this limit, the extraction of levels is somewhat arbitrary because of the high level density. An example of an experimental spectrum with the lineshape fit is shown in Fig. 1.

A DWBA analysis of the measured form factors was performed in order to extract the transition charge densities in the form of Fourier–Bessel expansion coefficients [14,15]. A cut-off radius R_c of 11 fm was chosen, which allows a reasonable number of parameters and avoids unphysical oscillations outside the nuclear radius. This last problem is also overcome, when necessary, by adding a tail bias [14,15] exponentially decreasing with r, to the transition charge density. This expansion is complete, so in principle this method is model independent. However, the transferred momentum range has an experimental upper limit of ~ 2.15 fm^{-1}, necessitating the assumption [16] of an exponentially decreasing cross section beyond $q_{\max}$. With this procedure up to nine Fourier–Bessel coefficients were fitted, due to the limited q-range. The lack of experimental points at higher momentum transfer in this experiment implies a reduced reliability of the densities at small radii, compared to those measured [5–7] previously. A few examples of form-factor data and DWBA fits are shown in Fig. 2, in which the high-q upper limits are also shown as dash–dotted curves.

In Table 1 the observed levels are listed by excitation energy; the assigned spin is indicated in the second column. The extracted reduced transition probability

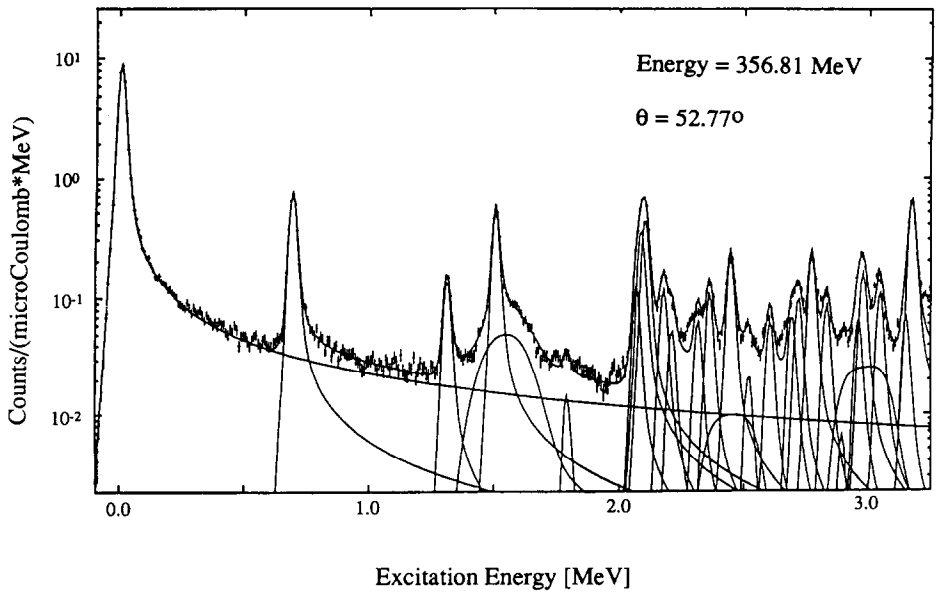

Fig. 1. A spectrum for inelastic electron scattering off ^{144}Nd taken at a momentum transfer of $q_{\text{eff}} = 1.85$ fm^{-1}. The curves indicate fits to the data (see text for details).

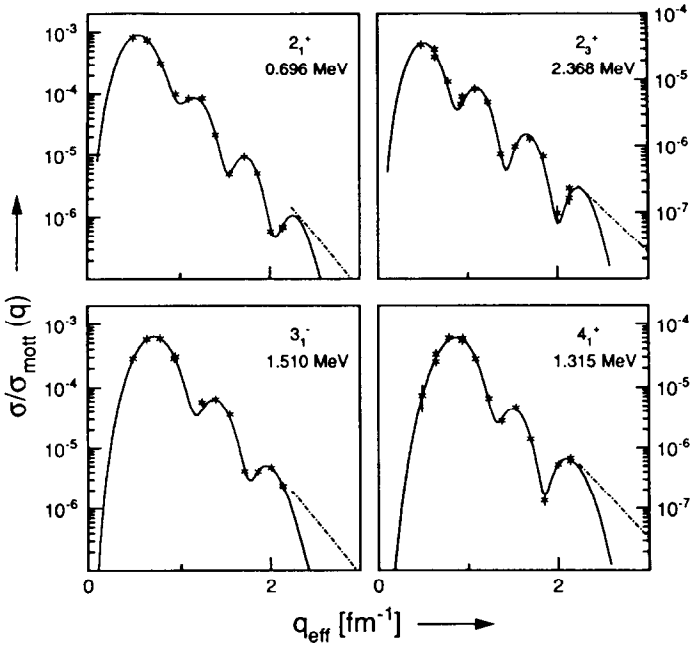

Fig. 2. Measured form factors for inelastic electron scattering for some states in ^{144}Nd observed in this work. The curves represent Fourier–Bessel fits.

Table 1
Excitation energies E_x, spins and parities J^π, and transition probabilities $B(E\lambda)$ of the excited states of ^{144}Nd as measured in this experiment and in ref. [9]

Present (e,e') work			(p,p'), (d,d') from ref. [9]		
E_x [MeV]	J^π	$B(E\lambda)$ $[e^2fm^{2\lambda}]$	E_x [MeV]	J^π	$B(E\lambda)$ [a] $[e^2fm^{2\lambda}]$
0.696	2^+	$4.60(40)\cdot10^3$	0.696	2^+	$5.37(20)\cdot10^3$
1.315	4^+	$1.93(27)\cdot10^6$	1.314	4^+	$3.40(34)\cdot10^6$
1.510	3^-	$2.56(20)\cdot10^5$	1.510	3^-	$2.92(16)\cdot10^5$
			1.561	2^+	$7.5(4)\cdot10^1$
			1.791	6^+	$1.83(17)\cdot10^8$
2.073	2^+	$6.31(34)\cdot10^2$	2.073	2^+	$4.20(25)\cdot10^2$
2.093	5^-	$0.94(26)\cdot10^8$	2.093	5^-	$1.52(15)\cdot10^8$
2.109	4^+	$3.14(39)\cdot10^6$	2.109	4^+	$3.36(32)\cdot10^6$
			2.185	1^-	$0.91(18)\cdot10^3$ [b]
2.218	6^+	$5.2(1.8)\cdot10^9$	2.217	(6^+)	$3.75(70)\cdot10^9$
			2.295	4^+	$1.30(3)\cdot10^6$
			2.327	$0+$	2.7(5) [c]
2.368	2^+	$2.38(21)\cdot10^2$	2.367	2^+	$2.24(10)\cdot10^2$
2.451	4^+	$1.13(17)\cdot10^6$	2.451	4^+	$6.5(7)\cdot10^5$
2.527	2^+	$3.47(34)\cdot10^2$	2.527	2^+	$3.47(17)\cdot10^2$
			2.590	(1^-)	$2.69(52)\cdot10^2$ [b]
			2.606		
			2.675	$(0+)$	1.7(3) [c]
			2.693	2^+	$3.7(4)\cdot10^1$
			2.717	(1^-)	$2.05(40)\cdot10^2$ [b]
2.779	3^-	$4.4(6)\cdot10^4$	2.779	3^-	$6.3(6)\cdot10^4$
2.839	3^-	$0.46(9)\cdot10^4$	2.833	3^-	$1.0(1)\cdot10^4$
			2.898	2^+	$4.3(4)\cdot10^1$
2.967	3^-	$8.1(1.1)\cdot10^3$	2.969	3^-	$8.40(84)\cdot10^3$
2.986	4^+	$6.9(1.2)\cdot10^5$	2.987	4^+	$7.8(9)\cdot10^5$
			3.026	5^-	$3.0(3)\cdot10^7$
3.053	5^-	$1.29(26)\cdot10^8$	3.049	5^-	$1.48(16)\cdot10^8$
			3.130	1^-	$1.80(80)\cdot10^2$ [b]
			3.180	(6^+)	$1.33(19)\cdot10^9$
			3.214	3^-	$2.31(26)\cdot10^3$
			3.240	(3^-)	$1.41(26)\cdot10^3$
			3.289	(3^-)	$4.12(60)\cdot10^3$
			3.340	4^+	$3.10(37)\cdot10^5$
			3.382	(4^+)	$2.72(32)\cdot10^5$
			3.401	5^-	$2.11(42)\cdot10^7$
			3.461	4^+	$2.04(36)\cdot10^5$
			3.493	5^-	$2.64(22)\cdot10^7$
			3.522	2^+	$0.93(18)\cdot10^2$
			3.555	2^+	$5.74(91)\cdot10^1$
			3.658	3^-	$4.52(65)\cdot10^3$

[a] The $B(E\lambda)$ values of ref. [9] refer to the isoscalar components of the excitations.
[b] In units of $[e^2fm^6]$.
[c] In units of $[e^2fm^4]$.

$B(\mathrm{E}\lambda)$ from the $J_i^\pi = 0^+$ ground state is reported in the third column; it is in general defined as:

$$B(\mathrm{E}\lambda) = \frac{(2J_f + 1)}{(2J_i + 1)} |M(\mathrm{E}\lambda)|^2, \tag{1}$$

where the 2^λ-pole moment $M(\mathrm{E}\lambda)$ is related to the transition charge density by the equation:

$$M(\mathrm{E}\lambda) = \int \rho_\lambda(r) r^{\lambda+2} \, \mathrm{d}r. \tag{2}$$

Similar results from a recent (p,p') and (d,d') measurement [9] are reported in the right side of the same table. These will be compared to the (e,e') results in more detail in sect. 4.

3. The quasiparticle-phonon model

The quasiparticle–phonon model [8] (QPM) is based on the construction of a phonon basis, where the phonons are defined as solutions of the quasiparticle-RPA equations. Starting from this basis, two- and multiple-phonon states are constructed. The spectrum of the nuclear excitations is then described by coupling one- and multiple-phonon states. Because of its microscopic foundations, the QPM consistently takes into account the interplay between collective and single-particle modes of excitation.

The general hamiltonian of the QPM is usually written as:

$$H = H_{\mathrm{sp}} + H_{\mathrm{pair}} + H_{\mathrm{m}} + H_{\mathrm{sm}}, \tag{3}$$

where H_{sp} is the single-particle hamiltonian, H_{pair} is the monopole pairing interaction, H_{m} is the separable multipole interaction in the particle–hole (ph) channel, and H_{sm} is the separable spin–multipole interaction in the ph channel. This hamiltonian is diagonalized in a few steps in the QPM. In the first step, a part of it, $H_{\mathrm{sp}} + H_{\mathrm{pair}}$, is diagonalized in the BCS formalism. Next, phonons are constructed as a linear combination of pairs of quasiparticles. For phonons the RPA equations are solved with the full hamiltonian of Eq. (3). Once the phonon basis is obtained, the QPM wave function of an excited state is written as a mixture of one-, two- and multiple-phonon terms (up to three-phonon terms in the present calculations) and the hamiltonian of Eq. (3) is diagonalized in the set of these wave functions. This yields the spectrum of the QPM excited states and the contributions of different phonon terms to their wave functions. The QPM formalism is presented in more details in refs. [5,8].

In treating the system of interacting phonons, we ignore the underlying fermion properties of the nuclear system, including the Pauli principle, because we are now

dealing with a system of bosons. This leads to an overdetermination of the many-phonon basis compared to the correctly antisymmetrized many-quasiparticle basis. This results in many spurious states [17]. Furthermore, the violation of the Pauli principle requires a renormalization of the matrix elements of the quasiparticle–phonon interaction. The Pauli principle is accounted for by adopting the so-called diagonalization approximation [8,17], which simplifies the calculation without loss of rigour.

After diagonalizing the hamiltonian of Eq. (3), transition charge densities can be calculated. If ground-state correlations are neglected, only one-phonon $\rho_i^J(r)$ and two-phonon $\rho_{\lambda i\lambda' i'}^J(r)$ densities contribute to the transition charge densities $\rho_\nu^J(r)$, as follows:

$$\rho_\nu^J(r) = \sum_i R_i(J\nu)\rho_i^J(r) + \sum_{\lambda i\lambda' i'} P_{\lambda i}^{\lambda' i'}(J\nu)\rho_{\lambda i\lambda' i'}^J(r), \tag{4}$$

where ν is the root number, J the total angular momentum, and $\rho_i^J(r)$ and $\rho_{\lambda i\lambda' i'}^J(r)$ are expressed in terms of the two-quasiparticle transition charge densities which take the form given in ref. [18]. Finally, to allow a comparison of the calculated transition densities with the experimental ones, the $\rho_\nu^J(r)$ are folded with the proton charge density which is parametrized according to ref. [19].

The parameters, which appear in the present calculations, were determined in the following way. We have used the same values of the parameters for the average field $H_{\rm sp}$ and pairing interaction $H_{\rm pair}$ as in calculations for ^{142}Nd (ref. [5]) and ^{146}Nd (ref. [6]) assuming that these parts of the hamiltonian do not change strongly within the Nd chain. The parameters of the residual interaction $H_{\rm m}$ have been adjusted to the properties of the lowest collective levels. The single-particle hamiltonian includes a Woods–Saxon potential with radial parameters $r_0 = 1.30$ fm, $a_0 = 0.55$ fm for protons [20], and $r_0 = 1.27$ fm, $a_0 = 0.62$ fm for neutrons [21]. All bound and narrow quasi-bound states, a total of 28 neutron levels and 29 proton levels with $j \leqslant \frac{19}{2}$, were included in the calculations. The model-independent energy-weighted sum rule [22] is reproduced by this single-particle spectrum for low J^π. Therefore, no effective polarisation charges are considered to be necessary, i.e. $e_Z = 1$ and $e_N = 0$ have been used.

Pairing correlations are treated in the BCS approximation with a constant value for the matrix element of the monopole pairing interaction in the particle–particle channel ($G \sim 17/A$ MeV).

4. Comparison between theory and experiment

4.1. The quadrupole states

The quasiparticle-RPA calculations predict eight 2^+ one-phonon states below $E_x = 4$ MeV. In Table 2 their predicted excitation energies, B(E2) values, and the

Table 2
Quadrupole–phonon configurations predicted by the quasiparticle-RPA calculations for ^{144}Nd

RPA state	E_x [MeV]	B(E2) [e^2fm^4]	Main 2qp configurations	
2_1^+	1.480	$4.4 \cdot 10^3$	$\nu(2f_{7/2}\,2f_{7/2})$	42%
			$\pi(2d_{5/2}\,2d_{5/2})$	23%
			$\pi(1g_{7/2}\,1g_{7/2})$	10%
2_2^+	2.308	$2.4 \cdot 10^2$	$\nu(2f_{7/2}\,2f_{7/2})$	43%
			$\pi(2d_{5/2}\,2d_{5/2})$	55%
2_3^+	2.502	$9.9 \cdot 10^1$	$\nu(2f_{7/2}\,2f_{7/2})$	5%
			$\pi(1g_{7/2}\,2d_{5/2})$	81%
2_4^+	2.261	$3.2 \cdot 10^2$	$\nu(2f_{7/2}\,2f_{7/2})$	5%
			$\pi(1g_{7/2}\,1g_{7/2})$	71%
			$\pi(1g_{7/2}\,2d_{5/2})$	14%
2_5^+	3.301	$1.1 \cdot 10^3$	$\nu(2f_{7/2}\,3p_{3/2})$	10%
			$\pi(1g_{7/2}\,1g_{7/2})$	13%
			$\pi(1h_{11/2}\,1h_{11/2})$	11%
			$\pi(1g_{7/2}\,2d_{3/2})$	21%
			$\pi(2d_{5/2}\,3s_{1/2})$	14%
2_6^+	3.597	$4.8 \cdot 10^1$	$\nu(2f_{7/2}\,1h_{9/2})$	95%
			$\pi(2d_{5/2}\,2d_{3/2})$	1%
2_7^+	3.831	$1.2 \cdot 10^0$	$\nu(2f_{7/2}\,3p_{3/2})$	1%
			$\pi(2d_{5/2}\,2d_{3/2})$	90%
2_8^+	3.937	$6.9 \cdot 10^{-1}$	$\nu(2f_{7/2}\,3p_{3/2})$	2%
			$\pi(2d_{5/2}\,3s_{1/2})$	70%
			$\pi(1g_{7/2}\,2d_{3/2})$	23%

main two-quasiparticle (2qp) configurations are reported. For the first four 2^+ one-phonon states, the calculated transition charge densities are plotted in Fig. 3.

The 2_1^+ phonon state predicted by the quasiparticle-RPA is the most collective one with the largest B(E2) value. Both the first and the second 2^+ phonon state are formed by 2qp configurations with comparable neutron and proton contributions. The higher 2^+ phonon states are almost pure 2qp excitations and show less collectivity, with the exception of the 2_5^+ phonon state, which is formed by many 2qp contributions and has an enhanced B(E2) value, only four times smaller than that of the 2_1^+ phonon state. The collectivity of the first four 2^+ phonon states can also be inferred from the shapes of the calculated transition charge densities predicted by the RPA in Fig. 3. The transition charge density of the 2_1^+ level is essentially peaked at the nuclear surface, whereas that of the 2_2^+ one shows a strong peak in the nuclear interior and a small surface contribution. The 2_3^+ phonon density shows a second derivative form, and the 2_4^+ density has the outer peak clearly pushed inside the nuclear radius.

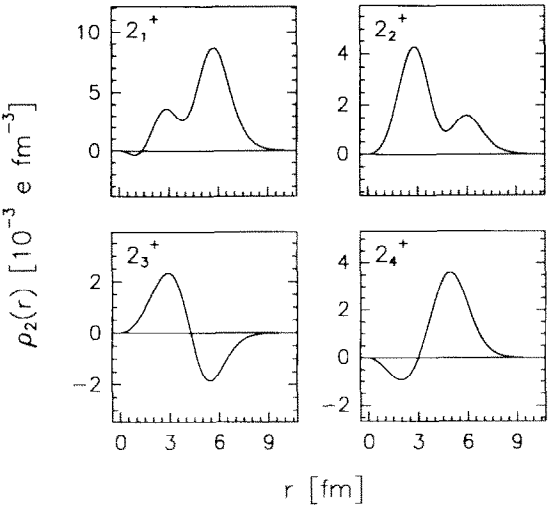

Fig. 3. Transition charge densities resulting from the RPA calculations for the first four quadrupole phonon states in ^{144}Nd.

We note that the 2_3^+, 2_4^+, 2_7^+, and 2_8^+ phonon states consist of almost pure proton configurations, whereas the other lower 2^+ phonon states have enhanced neutron configurations. This emphasizes the role played by the two valence neutrons outside the $N = 82$ closed shell.

The coupling of one-, two- and three-phonon configurations performed in the QPM approximation, pulls down the excitation energies of the quadrupole states (see Table 3). A comparison between the experimental excitation energies and B(E2) values with the same quantities predicted by the QPM is made in the upper part of Fig. 4. The 2_1^+ state predicted by the QPM calculations is mainly built up from the 2_1^+ RPA one-phonon configuration (78%); the two- and three-phonon components amount to 14% and 2%, respectively. The 2_2^+ state at $E_x = 1.575$ MeV is mainly a $[2_1^+ \otimes 2_1^+]$ two-quadrupole phonon excitation (63%), with a small ($\sim 10\%$) 2_2^+ one-phonon contribution.

The two-phonon contribution in the 2^+ states predicted for ^{144}Nd by the QPM is always greater than 10%, with the exception of the almost pure one-phonon states 2_4^+, 2_5^+ and 2_9^+. The transition charge densities of the most important two-phonon contributions $[2_1^+ \otimes 2_1^+]^{(2)}$, $[3_1^- \otimes 3_1^-]^{(2)}$ and $[2_1^+ \otimes 4_1^+]^{(2)}$ in the quadrupole excitations are shown in Fig. 5. In many 2^+ states the contribution of the three-phonon part is also strong ($\geqslant 10\%$). This situation is in contrast to the low-lying 2^+ states predicted [5] by the QPM for ^{142}Nd, where the two-phonon contribution is limited to only a few percent and the three-phonon component is negligible. This situation in ^{144}Nd results from the neutron pair outside the closed $N = 82$ core, which appreciably increases the coupling with the two-phonon and three-phonon parts of the QPM hamiltonian. This produces a more complicated

Table 3
Quadrupole excitations of ^{144}Nd predicted by the QPM calculations described in the text

QPM state	E_x [MeV]	B(E2) [e^2fm^4]	one-phonon component		two-phonon component		three-phonon component
2_1^+	0.708	$3.8 \cdot 10^3$	2_1^+	78%	$2_1^+ \otimes 4_1^+$	6%	2%
					$3_1^- \otimes 3_1^-$	4%	
					$3_1^- \otimes 5_1^-$	4%	
2_2^+	1.575	$7.9 \cdot 10^1$	2_2^+	10%	$2_1^+ \otimes 2_1^+$	63%	19%
			2_4^+	4%			
2_3^+	2.105	$1.5 \cdot 10^2$	2_2^+	70%	$2_1^+ \otimes 2_1^+$	7%	5%
					$2_1^+ \otimes 4_1^+$	10%	
					$3_1^- \otimes 5_1^-$	2%	
2_4^+	2.440	$2.0 \cdot 10^2$	2_3^+	87%	$2_1^+ \otimes 4_1^+$	4%	2%
			2_4^+	2%			
2_5^+	2.528	$2.2 \cdot 10^2$	2_1^+	2%	$2_1^+ \otimes 4_1^+$	4%	2%
			2_3^+	6%	$2_1^+ \otimes 4_4^+$	3%	
			2_4^+	77%			
			2_5^+	3%			
2_6^+	2.864	$1.0 \cdot 10^2$	2_1^+	5%	$2_1^+ \otimes 2_1^+$	2%	15%
			2_2^+	10%	$2_1^+ \otimes 4_1^+$	40%	
			2_3^+	3%			
			2_4^+	11%			
			2_5^+	13%			
2_7^+	3.013	$1.1 \cdot 10^2$	2_1^+	2%	$2_1^+ \otimes 4_1^+$	8%	14%
			2_2^+	3%	$2_1^+ \otimes 4_5^+$	3%	
			2_5^+	44%	$3_1^- \otimes 3_1^-$	21%	
2_8^+	3.354	$3.6 \cdot 10^2$	2_5^+	20%	$2_1^+ \otimes 4_1^+$	3%	25%
			2_6^+	2%	$2_1^+ \otimes 4_5^+$	4%	
					$3_1^- \otimes 3_1^-$	35%	
					$3_1^- \otimes 5_1^-$	6%	
2_9^+	3.388	$8.6 \cdot 10^1$	2_5^+	2%	$2_1^+ \otimes 4_5^+$	2%	1%
			2_6^+	83%	$2_1^+ \otimes 4_6^+$	7%	

mixing and splitting among the configurations, and lowers the energy of the calculated quadrupole excitations. A situation similar to that of ^{144}Nd has been found [3] in ^{142}Ce, where compared to ^{140}Ce the additional neutron pair is responsible for the stronger interplay between the different components in the wave functions of excited states. The similarity between the experimental spectra of ^{144}Nd and ^{142}Ce obtained from electron-scattering experiments is illustrated in Fig. 6; the low-lying 2^+ states are displayed in the leftmost part of the figure.

Transition charge densities have been obtained for four levels in ^{144}Nd from electron scattering. Nine 2^+ states have been observed at an excitation energy below 3.7 MeV in (p,p') and (d,d') experiments [9]. The QPM also predicts nine

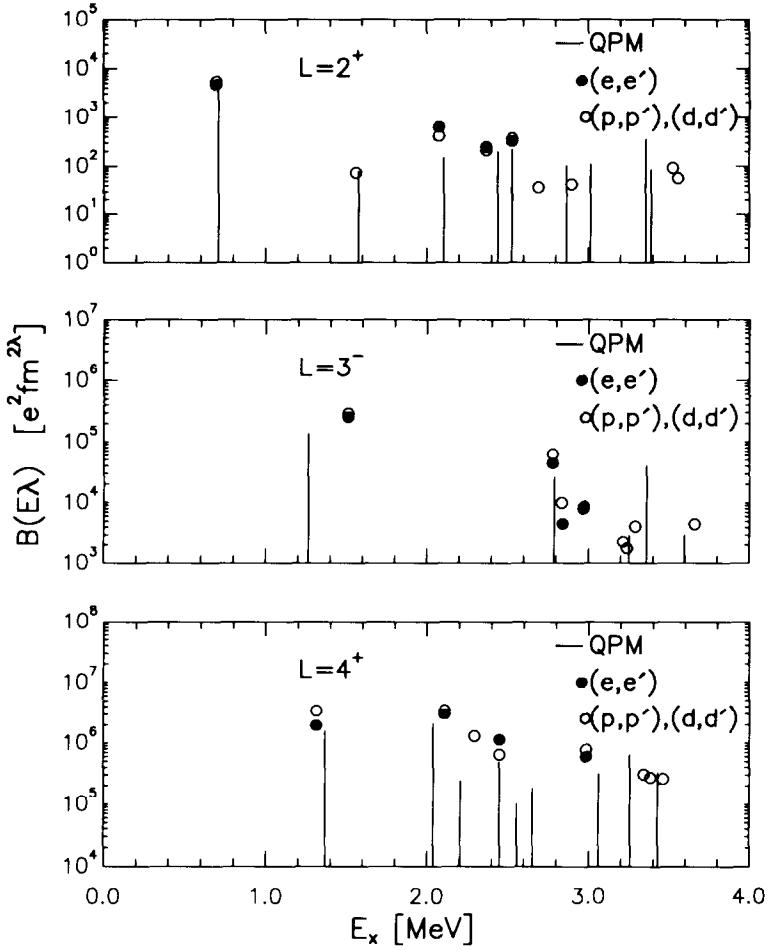

Fig. 4. Reduced transition probabilities for quadrupole (upper part), octupole (middle part), and hexadecapole (lower part) excitations in ^{144}Nd as determined in the present experiment (full circles), taken from ref. [9] (open circles) and calculated (vertical lines) by the QPM. For cases where the open circles overlap completely with the full circles, the former are difficult to notice (see Table 1 for more details).

2^+ levels in this energy range. As shown in the upper part of Fig. 4, the quadrupole strength distribution is reasonably well described by the QPM calculations. The measured transition charge densities are presented in Fig. 7.

The transition density of the 2_1^+ state at $E_x = 0.696$ MeV is nicely reproduced, although the QPM calculation overestimates the amplitude of the peak in the interior. The 2_2^+ state, known to be at $E_x = 1.561$ MeV, is not observed in the present electron-scattering experiment. This state has been observed in (p,p') and (d,d') experiments, where it is mainly excited by a two-step process via the 2_1^+ state. This suggests a very large two-phonon component for this state, as predicted

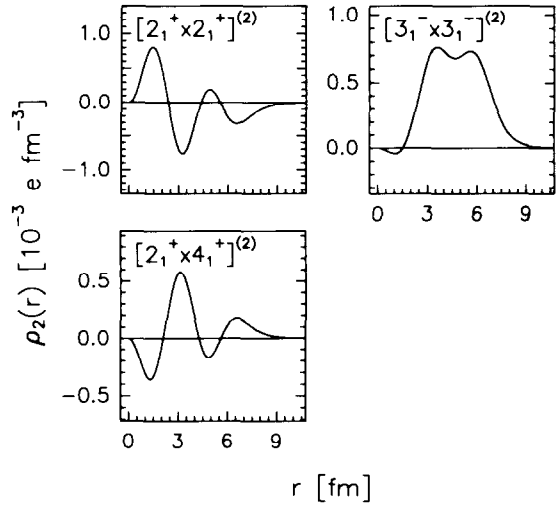

Fig. 5. Transition charge densities of some prominent two-phonon quadrupole configurations calculated in the QPM for ^{144}Nd.

by QPM calculations. In fact the model predicts for the 2_2^+ state at $E_x = 1.575$ MeV a 63% contribution from the two-phonon configuration $[2_1^+ \otimes 2_1^+]^{(2)}$. The 2_3^+ state, observed at 2.073 MeV, is predicted by the present calculations at 2.105 MeV. In this case, the calculation underestimates the B(E2) value by a factor of 4. The QPM 2_3^+ state has its main component (70%) from the second one-phonon 2^+ configuration. We note that the shapes of the experimental densities of the 2^+ states at 0.696 and 2.073 MeV are rather similar and very close to that of the calculated 2_1^+ state. This suggests that the experimental 2_3^+ state could arise from the splitting of the first RPA phonon and does not appear in the present

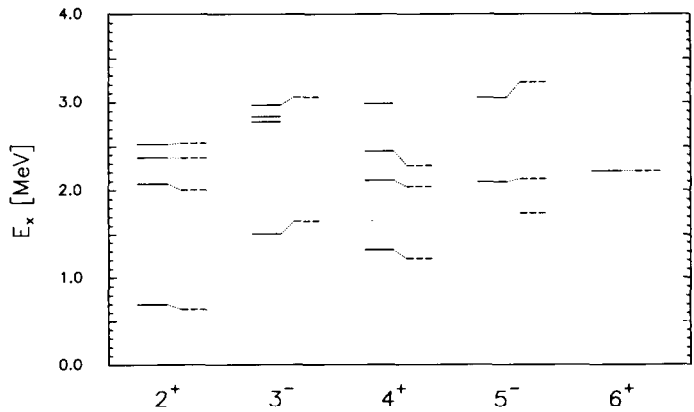

Fig. 6. Comparison of the energies of the levels excited by electron scattering in ^{144}Nd (full lines, present experiment) and ^{142}Ce (dashed lines, ref. [3]) for the indicated J^π states.

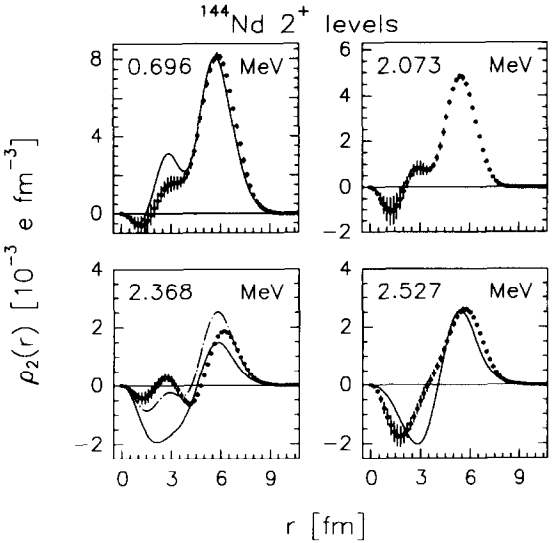

Fig. 7. Experimental quadrupole transition charge densities (full circles) of ^{144}Nd compared with the QPM calculations (curves). The predictions shown for the 2.368 MeV state are those for the 2_7^+ state (full curve) and 2_8^+ state (dot–dashed curve). The prediction shown for the 2.527 MeV state is that for the 2_4^+ state (full curve).

calculation due to the truncation of the basis used. The same remark has been made in ref. [3] in discussing the structure of the 2_3^+ state in ^{142}Ce.

The observed 2_4^+ and 2_5^+ states have excitation energies ($E_x = 2.368$ and 2.527 MeV, respectively) and B(E2) values in reasonable agreement with those predicted by the QPM calculation for the corresponding 2^+ states. However, the corresponding transition densities predicted by the QPM calculations do not agree with the data as well. The shape of the experimental transition charge density of the 2_5^+ state at $E_x = 2.527$ MeV is well reproduced by that of the calculated 2_4^+ level (full curve in Fig. 7), while the shape of the transition charge density of the 2_4^+ state at $E_x = 2.368$ MeV can only more or less be reproduced by those calculated in the QPM at about 700 keV higher in excitation energy, specifically at 3.013 and 3.354 MeV (the 2_7^+ and 2_8^+ states in the QPM calculation, reported in Fig. 7 with full and dot–dashed curves, respectively). These two 2^+ QPM states are the result of the fragmentation of the fifth RPA phonon (the most collective besides the first one) through mixing with two-phonon configurations (mainly the $[3_1^- \otimes 3_1^-]^{(2)}$ configuration). Expanding the phonon basis used in the present QPM calculations will affect mainly the collective phonons, with a stronger coupling to complex configurations. A full basis calculation should therefore split the fifth RPA quadrupole phonon and lower some fragment to excitation energies closer to that of the observed 2_4^+ state. A similar conjecture has also been formulated in the interpretation of the ^{142}Ce electron scattering data.

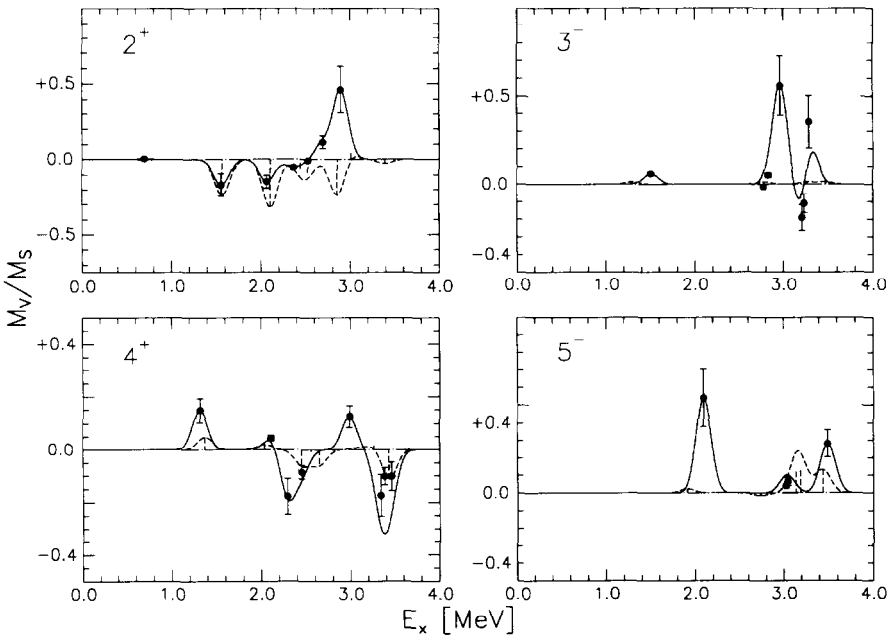

Fig. 8. Ratios of the isovector to isoscalar matrix elements in ^{144}Nd from ref. [9] (full circles with error bars and full curves), compared to the QPM evaluations (dashed vertical lines and dashed curves). Ratios for the 2^+ states at 3.522 and 3.555 MeV, the 3^- state at 3.658 MeV and the 5^- state at 3.401 MeV are missing because of lack of (d,d') data.

The coupling of the different RPA phonons to generate the QPM 2^+ states leads to a mixing of the isoscalar and isovector modes. This effect, caused by the quasiparticle–phonon interaction in the $N = 82$ isotones, has been recently stressed in ref. [23]. A useful quantity that highlights the neutron–proton asymmetry is the ratio M_V/M_S between the isovector and the isoscalar components of the transition multipole moment. This ratio has been deduced in ref. [9] by means of two probes (proton and deuteron) with different isospin with the relation $M_V/M_S = 2(M_{pp'} - M_{dd'})/M_{dd'}$. It can be evaluated by QPM with $M_V/M_S = (M_n - M_p)/(M_n + M_p)$. The comparison between the experimental and the predicted M_V/M_S values for the 2^+ states of ^{144}Nd is displayed in the upper part of Fig. 8. The experimental points (full circles with error bars) and the QPM values (vertical dashed lines) have been smeared with a gaussian of 200 keV width (full and dashed curves, respectively). The theoretical predictions are negative over the whole energy range explored (except for the 2_7^+ state at 3.013 MeV, which has a small positive M_V/M_S ratio that is hardly visible in Fig. 8), thus indicating a proton character for the 2^+ states. The measured M_V/M_S values are also negative up to 2.5 MeV, but with a smaller absolute value, and change sign beyond this excitation energy, thus suggesting a stronger neutron contribution.

Table 4
Octupole–phonon configurations predicted by the quasiparticle-RPA calculations for ^{144}Nd

RPA state	E_x [MeV]	B(E3) [e^2fm^6]	Main 2qp configurations	
3_1^-	2.350	$2.3 \cdot 10^5$	$\nu(2f_{7/2}\,1i_{13/2})$	10%
			$\nu(1h_{11/2}\,1i_{13/2})$	3%
			$\pi(2d_{5/2}\,1h_{11/2})$	69%
			$\pi(1g_{7/2}\,1h_{11/2})$	5%
			$\pi(1g_{9/2}\,1h_{11/2})$	2%
3_2^-	3.369	$9.8 \cdot 10^2$	$\nu(2f_{7/2}\,1i_{13/2})$	0.2%
			$\pi(1g_{7/2}\,1h_{11/2})$	91%

4.2. The octupole states

The quasiparticle RPA predicts for ^{144}Nd two octupole phonons below 4 MeV (Table 4). These phonons, at $E_x = 2.350$ MeV and $E_x = 3.369$ MeV, are mainly built up from proton 2qp configurations ($\sim 76\%$ and $\sim 91\%$, respectively). This feature makes the RPA-predicted octupole strength in ^{144}Nd very similar to that of ^{142}Nd, in contrast to the quadrupole and hexadecapole strengths (see also next section).

The first quasiparticle-RPA octupole phonon in ^{144}Nd is rather collective, because of the coherent mixing between different two-quasiparticle configurations. The second octupole phonon has a nearly pure 2qp nature, and, as a consequence, a less collective character, which is illustrated by the B(E3) values given in Table 4.

The coupling of one-, two- and three-phonon configurations in the QPM approximation, increases the number of 3^- states predicted below 4 MeV to five (Table 5). A reasonable agreement is observed between the QPM calculations and the measured excitation energies and B(E3) values (see the central part of Fig. 4). The degree of mixing between one-, two- and three-phonon configurations is rather strong in all octupole states (Table 5). In the 3_1^- level the one-phonon component is dominant (56%), but the two-phonon term already amounts to 31%, and the percentage of three-phonon configurations is 7%. All other 3^- states have a strong contribution from two-phonon configurations (up to 60% in the 3_2^- and 3_3^- states) and a three-phonon contribution larger than 15%.

Four 3^- states below 3 MeV have been observed in the (e,e') experiment, whereas six (and possibly eight) 3^- states have been observed below 3.7 MeV in the (p,p') and (d,d') experiments. The above eight 3^- states have to be compared with five 3^-states predicted by the QPM calculations. These calculations reproduce the overall structure of the experimental octupole strength distribution, as shown in Fig. 4. The comparison between the experimental and the calculated octupole transition densities is given in Fig. 9. It is worth noting that the transitions to the different final states have transition densities, both in the experiment and in

Table 5
Octupole excitations of ^{144}Nd predicted by the QPM calculations described in the text

QPM state	E_x [MeV]	B(E3) [e^2fm^6]	one-phonon component		two-phonon component		three-phonon component
3_1^-	1.265	$1.4 \cdot 10^5$	3_1^-	56%	$2_1^+ \otimes 3_1^-$	26%	7%
			3_2^-	2%	$2_1^+ \otimes 5_1^-$	5%	
3_2^-	2.787	$2.6 \cdot 10^4$	3_1^-	12%	$2_1^+ \otimes 3_1^-$	36%	27%
					$2_1^+ \otimes 5_1^-$	22%	
3_3^-	3.252	$3.0 \cdot 10^3$	3_1^-	5%	$2_1^+ \otimes 5_1^-$	20%	26%
			3_2^-	7%	$3_1^- \otimes 4_1^+$	39	
3_4^-	3.359	$4.1 \cdot 10^4$	3_1^-	13%	$2_1^+ \otimes 3_3^-$	3%	15%
			3_2^-	33%	$2_2^+ \otimes 3_1^-$	2%	
					$2_1^+ \otimes 5_1^-$	6%	
					$3_1^- \otimes 4_3^+$	25%	
3_5^-	3.596	$0.3 \cdot 10^4$	3_1^-	4%	$2_1^+ \otimes 3_1^-$	4%	18%
			3_2^-	33%	$2_1^+ \otimes 3_3^-$	7%	
					$2_1^+ \otimes 5_1^-$	16%	
					$2_1^+ \otimes 5_3^-$	2%	
					$3_1^- \otimes 4_1^+$	4%	
					$4_1^+ \otimes 5_1^-$	9%	

the calculation, with very similar shapes. Therefore correspondence between the observed and the QPM 3^- states has to be tested on the observed excitation energies and the measured trend of B(E3) values.

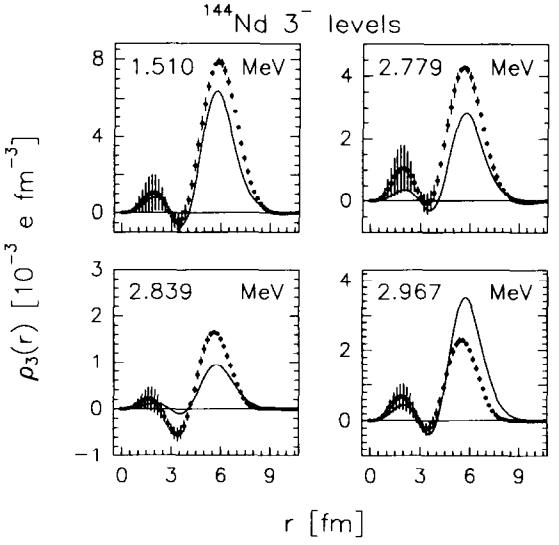

Fig. 9. Experimental octupole transition charge densities (full circles) of ^{144}Nd compared with the QPM calculations (curves).

In Fig. 9, the transition charge densities of the 3_1^-, 3_2^- and 3_3^- experimental states (at 1.510, 2.779 and 2.839 MeV, respectively) are compared with the QPM 3^- states (at 1.265, 2.787 and 3.252 MeV). The calculation reproduces reasonably well the excitation energy and the shape, but not the absolute value of the transition densities, which are somewhat underestimated. This is not the case for the 3_4^- state (located at 2.967 MeV but predicted at 3.359 MeV in the QPM calculation). The relatively strong transition leading to the 3_4^- state in QPM could account, however, for the summed strength of the multiplet of 3^- states observed at 2.967, 3.214, 3.240 and 3.289 MeV. The 3_5^- QPM state at 3.596 MeV could be identified instead, as far as excitation energy and strength are concerned, with the observed 3_8^- state at 3.658 MeV.

The effect of the mixing between isovector and isoscalar components of the 3^- states due to the quasiparticle–phonon interaction in ^{144}Nd is displayed in the second part of Fig. 8, where the calculated M_V/M_S ratio is compared to that measured in ref. [9]. The M_V/M_S values predicted by the QPM are almost all zero. This is in agreement with the experimental results, except for the strong neutron components in the 3^- levels at $E_x = 2.969$ and 3.290 MeV.

4.3. The hexadecapole states

The hexadecapole phonons predicted by the quasiparticle-RPA calculation below 4 MeV are listed in Table 6. The 4_2^+, 4_3^+, 4_4^+ and 4_7^+ phonons have predominant proton contributions. The 4_1^+ phonon has a dominant neutron contribution whereas the 4_5^+ and 4_6^+ phonons are mixed neutron and proton 2qp states. The excitation energies and the B(E4) values predicted by the QPM calculation for the nine $L = 4$ transitions are given in Table 7.

Four 4^+ states have been observed in electron scattering with excitation energies below 3 MeV and a total of seven (possibly eight) states below 3.7 MeV in proton scattering (Table 1). A comparison of QPM predictions with the experimental results is given in the lower part of Fig. 4. The excitation energies are reasonably well reproduced.

The 4_1^+ phonon predicted by the RPA is mainly (73%) based on the $(2f_{7/2}\,2f_{7/2})$ neutron two-quasiparticle configuration, which results in a non-collective nature. This phonon contributes with 40% and 45% to the 4_1^+ and 4_2^+ states in QPM, respectively. Its strength is split by mixing with the two-phonon configuration: $[2_1^+ \otimes 2_1^+]^{(4)}$. It is worth noting that in QPM the structure of the 4_1^+ state is strongly affected by the mixing between one- and two-phonon configurations. In ^{142}Nd, the lowest two-phonon configuration, $[2_1^+ \otimes 2_1^+]$, lies in excitation energy much higher than the 4_1^+ phonon. This results in a pure one-phonon configuration for the 4_1^+ state whereas the two-phonon configuration $[2_1^+ \otimes 2_1^+]^{(4)}$ mixes with the 4_4^+ phonon, which gives the 4_4^+ and the 4_5^+ states. In ^{144}Nd, as mentioned above, the mixing with the same two-phonon configuration splits the 4_1^+ phonon and yields the

Table 6
Hexadecapole–phonon configurations predicted by the quasiparticle-RPA calculations for ^{144}Nd

RPA state	E_x [MeV]	B(E4) [e^2fm^8]	Main 2qp configurations	
4_1^+	2.000	$2.8 \cdot 10^6$	$\nu(2f_{7/2}\,2f_{7/2})$	73%
			$\pi(2d_{5/2}\,2d_{5/2})$	13%
			$\pi(1g_{7/2}\,2d_{5/2})$	7%
4_2^+	2.307	$8.1 \cdot 10^5$	$\nu(2f_{7/2}\,2f_{7/2})$	21%
			$\pi(2d_{5/2}\,2d_{5/2})$	75%
			$\pi(1g_{7/2}\,2d_{5/2})$	3%
4_3^+	2.476	$6.3 \cdot 10^5$	$\nu(2f_{7/2}\,2f_{7/2})$	4%
			$\pi(1g_{7/2}\,2d_{5/2})$	81%
			$\pi(2d_{5/2}\,2d_{5/2})$	10%
			$\pi(1g_{7/2}\,1g_{7/2})$	3%
4_4^+	2.669	$4.2 \cdot 10^5$	$\nu(2f_{7/2}\,2f_{7/2})$	1%
			$\pi(1g_{7/2}\,1g_{7/2})$	90%
			$\pi(1g_{7/2}\,2d_{5/2})$	7%
4_5^+	3.483	$2.6 \cdot 10^6$	$\nu(2f_{7/2}\,1h_{9/2})$	42%
			$\nu(2f_{7/2}\,3p_{3/2})$	3%
			$\pi(2d_{5/2}\,2d_{3/2})$	27%
			$\pi(1h_{11/2}\,1h_{11/2})$	6%
			$\pi(1g_{7/2}\,2d_{3/2})$	7%
			$\pi(1g_{7/2}\,3s_{1/2})$	5%
			$\pi(1g_{7/2}\,1g_{7/2})$	2%
4_6^+	3.645	$1.3 \cdot 10^6$	$\nu(2f_{7/2}\,1h_{9/2})$	57%
			$\nu(2f_{7/2}\,3p_{3/2})$	3%
			$\pi(2d_{5/2}\,2d_{3/2})$	27%
			$\pi(1h_{11/2}\,1h_{11/2})$	3%
			$\pi(1g_{7/2}\,2d_{3/2})$	4%
			$\pi(1g_{7/2}\,3s_{1/2})$	2%
4_7^+	3.915	$1.6 \cdot 10^5$	$\nu(2f_{7/2}\,3p_{3/2})$	13%
			$\pi(2d_{5/2}\,2d_{3/2})$	40%
			$\pi(1g_{7/2}\,2d_{3/2})$	29%
			$\pi(1h_{11/2}\,1h_{11/2})$	11%
			$\pi(1g_{7/2}\,3s_{1/2})$	7%

experimental 4_1^+ and the 4_2^+ states. In ^{146}Nd, the 4_1^+ state is instead mostly a two-phonon state with a large three-phonon component (31%) and a small ($\leqslant 9\%$) one-phonon component [6]. In ^{144}Nd, strong two-phonon components are also present in other 4^+ states, with the exception of the 4_3^+ and 4_4^+ levels, which have almost pure one-phonon configurations.

Like for the other multipolarities the hexadecapole strength distribution (Fig. 4) is reasonably well described by the QPM calculation. The experimental transition charge densities, and those predicted by the QPM calculation, are displayed in Fig. 10. The transition charge densities of the 4_1^+, 4_2^+ and 4_4^+ states observed at 1.315,

Table 7
Hexadecapole excitations of ^{144}Nd predicted by the QPM calculations described in the text

QPM state	E_x [MeV]	B(E4) [e^2fm^8]	one-phonon component		two-phonon component		three-phonon component
4_1^+	1.368	$1.6 \cdot 10^6$	4_1^+	40%	$2_1^+ \otimes 2_1^+$	42%	12%
			4_5^+	2%			
4_2^+	2.039	$2.1 \cdot 10^6$	4_1^+	45%	$2_1^+ \otimes 2_1^+$	29%	12%
			4_2^+	5%			
4_3^+	2.207	$2.4 \cdot 10^5$	4_1^+	3%	$2_1^+ \otimes 2_1^+$	2%	2%
			4_2^+	84%	$2_1^+ \otimes 4_1^+$	4%	
4_4^+	2.449	$4.9 \cdot 10^5$	4_3^+	96%			
4_5^+	2.556	$1.0 \cdot 10^5$	4_2^+	5%	$2_1^+ \otimes 4_1^+$	47%	12%
			4_4^+	26%			
			4_5^+	2%			
			4_6^+	4%			
4_6^+	2.654	$1.8 \cdot 10^5$	4_4^+	70%	$2_1^+ \otimes 2_4^+$	2%	5%
			4_6^+	2%	$2_1^+ \otimes 4_1^+$	17%	
4_7^+	3.062	$3.2 \cdot 10^5$	4_1^+	2%	$2_1^+ \otimes 4_1^+$	2%	22%
			4_5^+	26%	$2_1^+ \otimes 6_1^+$	2%	
					$3_1^- \otimes 3_1^-$	41%	
4_8^+	3.256	$6.5 \cdot 10^5$	4_5^+	43%	$2_1^+ \otimes 2_5^+$	2%	14%
					$2_1^+ \otimes 6_1^+$	8%	
					$2_1^+ \otimes 6_4^+$	2%	
					$3_1^- \otimes 3_1^-$	22%	
					$3_1^- \otimes 5_1^-$	2%	
4_9^+	3.427	$3.3 \cdot 10^5$	4_5^+	2%	$2_1^+ \otimes 2_6^+$	4%	3%
			4_6^+	64%	$2_1^+ \otimes 4_1^+$	4%	
					$2_1^+ \otimes 6_1^+$	16%	
					$2_1^+ \otimes 6_4^+$	4%	

2.109 and 2.451 MeV are compared with those of the corresponding QPM states predicted at 1.368, 2.039 and 2.449 MeV, respectively. Based on the shape of the transition density and the B(E4) value of the 4_5^+ state observed at 2.986 MeV, its transition density is compared with that of the 4_8^+ QPM state at 3.256 MeV.

The mixing of one-phonon configurations and the presence of two- and three-phonon configurations in the hexadecapole excitations predicted by the QPM, reduces the proton component (dominant in the RPA calculations) in the wave functions of the 4_2^+, 4_3^+ and 4_4^+ levels. As a result of this, smaller values are obtained for the M_V/M_S ratio. This is illustrated in the third part of Fig. 8. This behaviour is in satisfactory agreement with the experimental results of ref. [9].

The excitation energies of the 4^+ states of ^{144}Nd are very similar to those of ^{142}Ce (central part of Fig. 6). Also the corresponding transition charge densities have similar shapes in both nuclei, although a closer look at the underlying

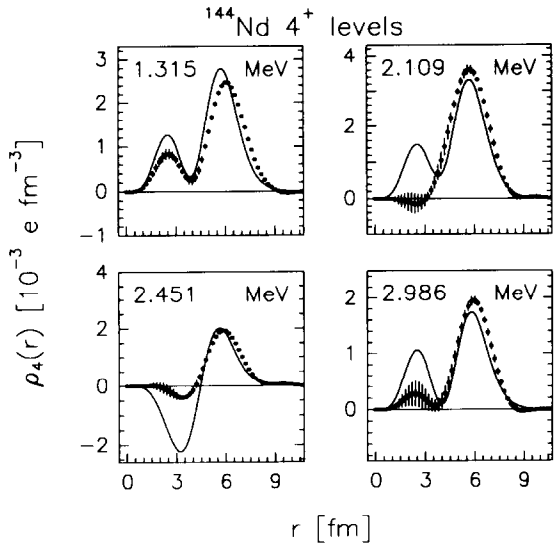

Fig. 10. Experimental hexadecapole transition charge densities (full circles) of ^{144}Nd compared with the QPM calculations (curves).

structure shows that different percentages of one- and two-phonon components contribute in the two nuclei.

4.4. States with higher multipolarity

In this experiment only three states with multipolarity different from $L = 2, 3, 4$ have been observed. These are two 5^- states at $E_x = 2.093$ MeV and $E_x = 3.053$ MeV, and one 6^+ state at $E_x = 2.218$ MeV. Their measured transition charge densities are shown in Fig. 11, where they are compared with the QPM predictions.

The quasiparticle-RPA calculation predicts two 5^- phonons below 4 MeV. They are mainly built up from proton 2qp configurations: the 5_1^- phonon at $E_x = 2.810$ MeV is formed by $\pi(2d_{5/2}\,1h_{11/2})$ (67%), $\pi(1g_{7/2}\,1h_{11/2})$ (18%) and $\nu(2f_{7/2}\,1i_{13/2})$ (5%) and the 5_2^- phonon at $E_x = 3.331$ MeV by $\pi(1g_{7/2}\,1h_{11/2})$ (75%) and $\pi(2d_{5/2}\,1h_{11/2})$ (24%), with a negligible neutron contribution.

The coupling of these one-phonon configurations with two- and three-phonon configurations gives rise in the QPM approximation to six 5^- states below 4 MeV. The lower-lying 5_1^-, 5_2^- and 5_3^- states display a strong mixing between the one- and two-phonon components. The main two-phonon components are $[2_1^+ \otimes 3_1^-]$ (40%) in the 5_1^- level, $[2_1^+ \otimes 3_1^-]$ (23%) and $[2_1^+ \otimes 5_1^-]$ (23%) in the 5_2^- level, and $[3_1^- \otimes 4_1^+]$ (45%) in the 5_3^- level. The 5_1^- RPA one-phonon component is strong in the 5_1^- QPM level. In spite of that, the strong proton character of the 5_1^- state, as calculated by the RPA, is diminished in QPM by the coupling to two- and

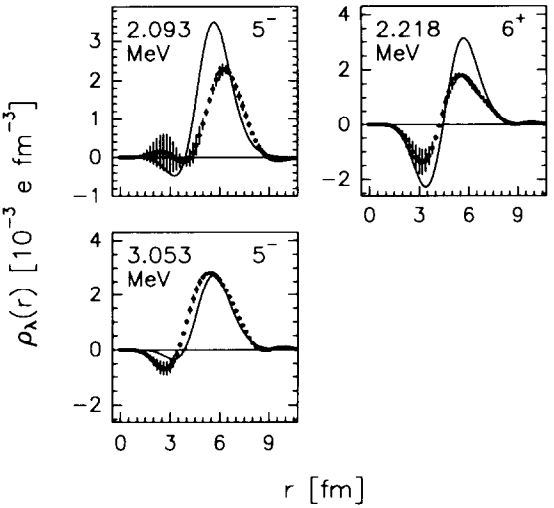

Fig. 11. Experimental transition charge densities (full circles) compared with the QPM calculations (curves) for the 5^- and 6^+ states observed in the present experiment for ^{144}Nd.

three-phonon configurations (lower part of Fig. 8). A value around zero is in fact predicted by the QPM for the M_V/M_S ratio of the 5_1^- level, whereas the experiment of ref. [9] gives indication of a strong neutron character for this level.

The 6_1^+ phonon calculated for ^{144}Nd by the quasiparticle-RPA is located at $E_x = 2.102$ MeV, and is mainly based on the $\nu(2f_{7/2}\,2f_{7/2})$ 2qp configuration (89%); the proton $\pi(1g_{7/2}\,2d_{5/2})$ 2qp configuration contributes only 9%. The higher-lying 6^+ RPA phonons are instead formed mainly by proton 2qp configurations. The only 6^+ state observed in the present work corresponds to the second 6^+ level predicted by the QPM calculations. The first 6^+ QPM state is located at $E_x = 1.822$ MeV, in good agreement with the state observed at $E_x = 1.791$ MeV in ref. [9]. The cross section of this level was below the detection limit for the present experiment. Both of these first two QPM 6^+ states are essentially built from one-phonon excitations. The first 6^+ state with a strong two-phonon component is predicted by the QPM at $E_x = 2.700$ MeV.

The 5_1^- level observed in ^{142}Ce has no counterpart in ^{144}Nd. Similarities among excitation energies and transition charge densities suggest that the first two 5^- states of ^{144}Nd have to be compared with the 5_2^- and the 5_3^- states of ^{142}Ce. In fact, the transition charge densities of the level at 2.093 MeV in ^{144}Nd and of the level at 2.125 MeV in ^{142}Ce are surface peaked, while those of the levels at 3.053 MeV in ^{144}Nd and at 3.222 MeV in ^{142}Ce have surface peaks that are pushed about 1 fm inward. The 6^+ state at 2.218 MeV in ^{144}Nd displays also a transition charge density that is similar in shape to that of the only 6^+ level observed [3] in ^{142}Ce at 2.220 MeV.

A final comment concerns the 5_1^- level. Controversial results have been reported in the literature [24–27] on the origin of this state in ^{144}Nd as well in other $N = 84$ isotones (Ba, Ce, Sm). In ref. [25] it has been suggested that the main component is a two-phonon (octupole–quadrupole) configuration and therefore that this state is essentially excited by a two-step process via the 2_1^+ and 3_1^- vibrational states. The validity of this conjecture would imply that the 5_1^- level should be hardly excited in high-energy electron scattering, which does not induce two-step excitations. Evidence of a strong direct excitation was already obtained by Cottle *et al.* [28] from the analysis of (p,p') data and is clearly established by the present experiment. In ref. [28], the $\nu(2f_{7/2}\,1i_{13/2})$ 2qp configuration has been suggested, as the main source of this strong direct coupling, whereas in electron scattering only the proton configurations contribute to the longitudinal form factor. A dominant neutron contribution is also suggested by the positive sign of the M_V/M_S ratio given in Fig. 8 for this state. RPA evaluations predict a dominant proton contribution, while QPM calculations give nearly equivalent proton and neutron contributions.

5. Summary and conclusions

In this paper the results of a high-resolution (12–30 keV) electron-scattering experiment on the ^{144}Nd isotope have been presented. A transferred-momentum range up to 2.15 fm^{-1} was covered. The excitation of many $J^\pi = 2^+$, 3^-, 4^+ and some 5^- and 6^+ states was observed below 3.1 MeV of excitation energy. For the observed states the transition charge densities have been extracted by means of a Fourier–Bessel analysis of the measured form factors.

The low-lying excitation modes of ^{144}Nd were investigated by comparing the experimental data with the predictions of QPM calculations. The comparison is intended to test the validity of the QPM, which satisfactorily reproduces [5] the radial structure of the low-lying excitations in the semi-magic nucleus ^{142}Nd, in the case that a neutron pair is added to the $N = 82$ shell closure. This test has already been performed in ref. [3] for the isotone ^{142}Ce.

A general good agreement between experiment and theory (QPM) has been found for ^{144}Nd. In particular, the quadrupole, octupole, and hexadecapole strength distributions are well described by the calculations, and a reasonable description of the transition charge densities is obtained. The lower-lying quadrupole states are mainly described by the QPM calculations as one-phonon excitations, with the exception of the 2_2^+ level, the main component of which is the $[2_1^+ \otimes 2_1^+]$ two-quadrupole phonon. The 2_1^+ level is the most collective quadrupole state in ^{144}Nd. This is confirmed both by the B(E2) value and the transition charge density, which is strongly surface peaked. An inner structure in the transition density is attributable to the $\pi(2d_{5/2}\,2d_{5/2})$ 2qp density, an effect already observed in ^{142}Nd.

The quadrupole excitations higher than the 2_2^+ state are predicted by the QPM to be almost pure proton configurations, a feature common to all quadrupole excitations of ^{142}Nd. Thus the effect of the two neutrons outside the $N = 82$ shell closure is mainly restricted to the first two quadrupole excitations of ^{144}Nd.

The microscopic structure of the hexadecapole excitations in ^{144}Nd is different from that of the quadrupole excitations. The 4_1^+ is collective because of a strong $[2_1^+ \otimes 2_1^+]$ two-quadrupole phonon contribution, coupled to a nearly pure neutron 2qp one-phonon component. The higher hexadecapole excitations display less collectivity, owing to interference between one- and two-phonon contributions with different underlying 2qp structure.

The influence of the neutron 2qp configurations is much less pronounced in the low-lying octupole excitations, thus making the octupole strength in ^{144}Nd very similar to that of ^{142}Nd, as far as the one-octupole phonon component is concerned. However, the presence of a strong two- and even three-phonon contribution makes the octupole strength of ^{144}Nd different from that of ^{142}Nd and more collective. The octupole transition charge densities are well reproduced in shape by the QPM calculations, but their magnitudes are somewhat underestimated.

The predominant proton or neutron character of the transitions calculated in RPA is deeply changed by the coupling between one-, two- and three-phonon configurations in QPM. In ^{144}Nd, the RPA calculations predict a major proton component in the excitations up to 3 MeV, whereas in the QPM calculations this character is counterbalanced by a significant neutron component in the quadrupole states, and an almost equal neutron component in the higher multipolarities. The experiment shows instead a slight neutron prevalence in only a few states.

Summarising, the QPM gives a satisfactory description of the excitation spectrum of ^{144}Nd. A detailed comparison between data and model predictions, however, indicated some shortcomings of the calculations performed. The excitation energies of some 2^+ states are not satisfactorily reproduced, the fragmentation of the octupole strength is underestimated, the transition probabilities, and in particular the neutron contribution to the transition strength, are slightly underestimated in some cases. This is usual for microscopic calculations with a truncated basis and without effective charges. The presence of a neutron pair outside the $N = 82$ shell closure makes the one-phonon components of the wave functions of the excited levels of ^{144}Nd more rich in neutron configurations compared to the nearly pure proton configurations in ^{142}Nd. This is similar to the situations observed in refs. [3,4] for ^{140}Ce and ^{142}Ce. The neutron pair is responsible also for the strong presence in the excited levels of ^{144}Nd of two- and three-phonon components; these are nearly absent in ^{142}Nd. The presence of multi-phonon configurations at low excitation energies increases with the collectivity of the nucleus and complicates the interpretation of low-lying states in the framework of the QPM.

This work is part of the research program of the Foundation for Fundamental Research of Matter (FOM), which is financially supported by the Netherlands' Organisation for Scientific Research (NWO).

References

[1] V. Meot, Ph.D. Thesis, University of Paris VII (1987), unpublished
[2] X.-H. Phan, H.G. Andresen, L.S. Cardman, J.-M. Cavedon, J.-C. Clemens, B. Frois, M. Girod, D. Gogny, B. Grammaticos, R. Hoffmann, M. Huet, P. Leconte, S.K. Platchkov, I. Sick and S.E. Williamson, Phys. Rev. C38 (1988) 1173
[3] W. Kim, J.R. Calarco, J.P. Connelly, J.H. Heisenberg, F.W. Hersman, T.E. Milliman, J.E. Wise, B.L. Miller, C.N. Papanicolas, V.Yu. Ponomarev, E.E. Saperstein and A.P. Platonov, Phys. Rev. C44 (1991) 2400
[4] W. Kim, B.L. Miller, J.R. Calarco, L.S. Cardman, J.P. Connelly, S.A. Fayans, B. Frois, D. Goutte, J.H. Heisenberg, F.W. Hersman, V. Meot, T.E. Milliman, P. Mueller, C.N. Papanicolas, A.P. Platonov, V.Yu. Ponomarev and J.E. Wise, Phys. Rev. C45 (1992) 2290
[5] R.K.J. Sandor, H.P. Blok, U. Garg, M.N. Harakeh, C.W. de Jager, V.Yu. Ponomarev, A.I. Vdovin and H. de Vries, Nucl. Phys. A535 (1991) 669; Phys. Lett. B233 (1989) 54;
R.K.J. Sandor, Ph.D. Thesis, Vrije Universiteit, Amsterdam (1991)
[6] R.K.J. Sandor, H.P. Blok, M. Girod, M.N. Harakeh, C.W. de Jager, V.Yu. Ponomarev and H. de Vries, Nucl. Phys. A551 (1993) 378
[7] R.K.J. Sandor, H.P. Blok, M. Girod, M.N. Harakeh, C.W. de Jager and H. de Vries, Nucl. Phys. A551 (1993) 349;
R.K.J. Sandor, H.P. Blok, U. Garg, M. Girod, M.N. Harakeh, C.W. de Jager and H. de Vries, Phys. Rev. C43 (1991) R2040
[8] V.G. Soloviev, Prog. Part. Nucl. Phys. 19 (1987) 107;
V.V. Voronov and V.G. Soloviev, Sov. J. Part. Nucl. 14 (1983) 583
[9] M. Pignanelli, N. Blasi, J.A. Bordewijk, R. De Leo, M.N. Harakeh, M.A. Hofstee, S. Micheletti, R. Perrino, V.Yu. Ponomarev, V.G. Soloviev, G. Sushkov and S.Y. van der Werf, to appear in Nucl. Phys. A
[10] C. de Vries, C.W. de Jager, L. Lapikás, G. Luijckx, R. Maas, H. de Vries and P.K.A. de Witt Huberts, Nucl. Instr. Meth. 233 (1984) 1
[11] A.J.C. Burghardt and W.T.A. Borghols, NIKHEF-K, internal report 84-A2 (1984), unpublished
[12] E.A.J.M. Offerman, Ph.D. Thesis, University of Amsterdam (1988), unpublished
[13] C.E. Hyde-Wright, Ph.D. Thesis, MIT (1984), unpublished;
J.J. Kelly, private communication
[14] J. Heisenberg, Adv. Nucl. Phys. 12 (1981) 61
[15] J. Heisenberg and H.P. Blok, Ann. Rev. Nucl. Part. Sci. 33 (1983) 596
[16] H. Rothhaas, J. Friedrich, K. Merle and B. Dreher, Phys. Lett. B51 (1974) 24
[17] V.G. Soloviev, Ch. Stoyanov and R. Nikolaeva, Bull. Acad. Sci. USSR, Phys. Ser. 47 (1983) 2082
[18] H.C. Lee, preprint of Chalk River Nuclear Laboratories, AECL-4839, Chalk River, Ontario (1975)
[19] G.G. Simon, C. Schmitt, F. Borkowski and V.H. Walther, Nucl. Phys. A333 (1980) 381
[20] J.B.J.M. Lanen, Ph.D. Thesis, University of Utrecht (1990), unpublished
[21] V.Yu. Ponomarev, V.G. Soloviev, Ch. Stoyanov and A.I. Vdovin, Nucl. Phys. A323 (1979) 446
[22] A.M. Bernstein, Advances in Nuclear Physics, vol. 3, ed. M. Baranger and E. Vogt (Plenum, New York, 1969) p. 321
[23] T.K. Dinh, M. Grinberg and C. Stoyanov, J. of Phys. G18 (1992) 329
[24] Ya.Ya. Berzin, M.R. Beitin, A.E. Kruminya, P.T. Prokof'ev, Kh. Rotter, Kh. Khaizer, F. Stari and V. Paar, Izv. Akad. Nauk SSSR 40 (1976) 1193
[25] P.D. Cottle, S.M. Aziz, J.D. Fox, K.W. Kemper and S.L. Tabor, Phys. Rev. C40 (1989) 2028
[26] C.H. King, B.A. Brown and T.-L. Khoo, Phys. Rev. C18 (1978) 2127
[27] S. Lunardi, P. Kleinheinz, M. Piiparinen, M. Ogawa, M. Lach and J. Blomqvist, Phys. Rev. Lett. 53 (1984) 1531
[28] P.D. Cottle, S.M. Aziz, K.W. Kemper, M.L. Owens, E.L. Reber, J.D. Brown, E.R. Jacobsen and Y.Y. Sharon, Phys. Rev. C42 (1990) 762